



Analysis of crosstalk in spectral beam-combining systems based on oscillation modes

Zhen Wu^{1,2} · Wei Cai¹ · Peng Feng¹ · Chengshuang Yang¹ · Yinghao Zhuang¹ · Qingsong Zhang¹ · Zairu Ma^{1,2}

Received: 16 May 2023 / Accepted: 26 June 2023 / Published online: 14 July 2023
© The Author(s), under exclusive licence to Springer-Verlag GmbH Germany, part of Springer Nature 2023

Abstract

The output spectra and combining efficiency of the spectral beam-combining (SBC) system are significantly affected by the crosstalk effect. An in-depth understanding of the oscillation modes of the diode lasers (DLs) and the crosstalk effect can enhance the SBC system. It is the first time that the relationship between locked spectral modes of the DLs and the crosstalk is built up. By dividing the crosstalk into self-crosstalk and mutual-crosstalk, the influence of crosstalk on the combining efficiency of the SBC system is analyzed based on the Lang–Kobayashi rate equations. Results indicate that the influence of self-crosstalk on the combining efficiency is weaker than that of the mutual-crosstalk. When the crosstalk factor is 0.2, the combining efficiency is only reduced by about 1.7% due to self-crosstalk, while the reduction in efficiency caused by mutual-crosstalk is up to 30%. In addition, for mutual-crosstalk, first-order crosstalk has a greater impact on efficiency than high-order crosstalk. The fourth-order crosstalk causes only a 3% decline in combining efficiency, while the first-order crosstalk results in a decrease of about 27%.

1 Introduction

Diode lasers have become a popular choice for light sources in various applications, including material processing, pump sources for solid-state lasers, and industrial manufacturing [1]. Recently, direct diode laser sources with high power and excellent beam quality have gained significant research interest [2]. However, due to the unique structures of diode lasers, their beam qualities tend to degrade as the power increases. Fortunately, a spectral beam-combining (SBC) method proposed by Lincoln Laboratory can effectively address this issue. The SBC system contains a diode laser array (DLA), a transform lens, a grating and an output coupler [3]. The grating provides wavelength-selective feedback and helps emitters to lock their wavelengths over their wide gain profiles [4]. However, a free-running diode laser always operates with a divergence angle, which can bring about beam crosstalk and mode hopping. The unwanted crosstalk and mode hopping inevitably affect the brightness of

the combined beam [5]. At present, many studies on the SBC technique have been performed. In 2017, Yang established a propagation model of crosstalk and found that beam crosstalk degraded combined power and beam quality [6]. Bochove found that adjacent emitters with sufficient interval suppressed crosstalk [7], but too large interval increased the spectral width of the combined beam [8]. Goyal introduced a spatial filter to successfully control the crosstalk in 2001, but this method sacrificed combined power [9]. In 2015, Huicheng Meng used a cylindrical coupler to collimate beams, which guaranteed that the backward beam was only fed back into the corresponding emitter [10]. Sevan's experiment proved that the combining efficiency was limited due to the thermal crosstalk [11]. Up to now, there have been lots of excellent studies of the SBC technique [12–15], which demonstrates that the SBC technique is a promising method to obtain laser beams with high brightness. Currently, the theoretical analysis of crosstalk phenomena lags behind experimental researches. We expect that a deep understanding of external-feedback lock can be helpful for practical applications of diode laser sources.

In this paper, the center wavelengths of the DLA are obtained by the grating equation, and their spectral modes are determined by the gain functions. Based on the spectral modes, we divide the crosstalk into self-crosstalk and mutual-crosstalk, and investigate their impact on the

✉ Zhen Wu
wuzhen@mail.xhu.edu.cn

¹ School of Science, Xihua University, Chengdu 610039, China

² Key Laboratory of Advanced Scientific Computation, Xihua University, Chengdu, China

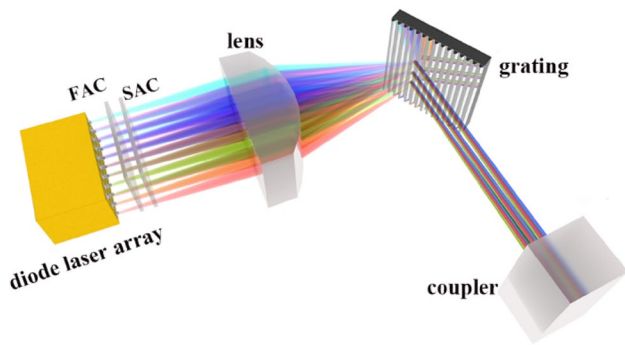


Fig. 1 The SBC system

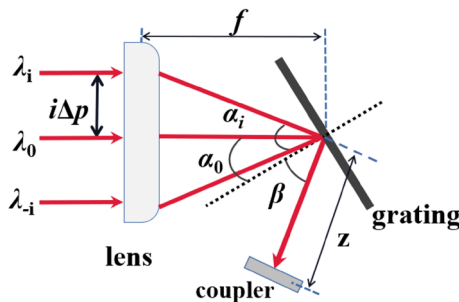


Fig. 2 Schematic of beams diffracted by the grating

combining efficiency using the Lang–Kobayashi rate equations.

2 The oscillation modes in the SBC structure

Figure 1 shows a schematic of a SBC system which mainly includes a DLA, a fast-axis collimator (FAC), a slow-axis collimator (SAC), a transform lens, a grating, and an output coupler. The transform lens is placed between the DLA and the grating with a focal length interval, and makes beams incident on the grating with different angles. Then, due to the dispersion effect of the grating, beams are incident on the coupler at the same angle. The SBC system can be simplified as a coupled cavity. The space between the front facet and the rear facet of an emitter functions as an internal cavity, and that between the front facet and the coupler is regarded as an external cavity. The locked spectra are subject to external cavity feedback. Due to the interaction between the two cavities, the wavelengths of the emitters are different from each other.

2.1 Calculation of the oscillation modes

Figure 2 shows beams diffracted by the grating. Emitters are symmetrically arranged at both sides of the central emitter,

and their wavelengths and incidence angles are $\lambda_i, \dots, \lambda_0, \dots, \lambda_{-i}, \alpha_i, \dots, \alpha_0, \dots, \alpha_{-i}$, respectively. The central beam falls on the grating at the Littrow angle:

$$\alpha_0 = \arcsin(\lambda_0/2d), \tag{1}$$

where d is the grating period. According to the geometrical relationship in Fig. 2, the incidence angle of the i th beam is obtained as

$$\alpha_i = \alpha_0 - \arctan\left(\frac{i\Delta p}{f}\right), i = 0, \pm 1, \dots, \tag{2}$$

where Δp is the interval between two adjacent emitters. f is the focal length of the lens. Due to the dispersion of the grating, the center wavelength of the i th emitter can be calculated as

$$\lambda_i = \lambda_0 + d \left[\sin\left(\alpha_0 - \arctan\left(\frac{i\Delta p}{f}\right)\right) - \sin\alpha_0 \right]. \tag{3}$$

The spectral modes can be analyzed using the multi-beam interference theory [16]. The internal cavity is treated as a Fabry–Perot resonator. Its rear facet is generally coated with high-reflection film, and its front facet is coated with anti-reflection film. Beams are reflected and amplified many times between the two facets. The main energy passes through the front facet. The two successively optical fields E_n and E_{n+1} meet the equation

$$E_{n+1} = G_m \sqrt{R_1 R_2} E_n e^{i\gamma}, \tag{4}$$

where R_1 and R_2 are the reflectances of the rear and front facets, respectively. R_1 is much higher than R_2 . $\gamma = 4\pi L_{ic}/\lambda + 2\pi$ is the phase shift of the wave propagation one-round trip in the internal cavity. L_{ic} is the length of the internal cavity. G_m is the one-round gain of the working medium. The field E_{ic} in the internal cavity is expressed as

$$E_{ic} = \sum_{n=1}^{\infty} E_n = \frac{\sqrt{G_m T_2} E_0}{1 - G_m \sqrt{R_1 R_2} e^{i\gamma}}, \tag{5}$$

where E_0 is the initial field. T_2 is the transmittance of the front facet. The optical intensity from the internal cavity can be given as

$$I_{ic} = |E_{ic}|^2 = \frac{G_m T_2}{1 + G_m^2 R_1 R_2 - 2G_m \sqrt{R_1 R_2} \cos\gamma} E_0^2. \tag{6}$$

Finally, the mode resonating in the internal cavity can be calculated as

$$G_{ic} = \frac{G_m}{1 + G_m^2 R_1 R_2 - 2G_m \sqrt{R_1 R_2} \cos\gamma}. \tag{7}$$

The mode does not only resonate in the internal cavity, and also resonates in the external cavity. In an analogous derivation procedure, the mode resonating in the external cavity is derived as

$$G_{ec}(R_g) = \frac{T_i T_2}{1 + G_m^2 T_i^2 T_2^2 R_1 R_g - 2G_m T_i T_2 \sqrt{R_1 R_g} \cos \beta_1}, \quad (8)$$

where $\beta_1 = 4\pi L_{ec}/\lambda + 2\pi$ represents the phase shift of the beam that travels a one-round trip in the external cavity. L_{ec} is the length of the external cavity. T_i is the transmittance of the lens, and R_g is the peak reflectance of the grating at the center wavelength λ_0 . Due to the grating selection, Eq. (8) is modified as

$$G_{ec}(R_3) = \frac{T_i T_2}{1 + G_m^2 T_i^2 T_2^2 R_1 R_3 - 2G_m T_i T_2 \sqrt{R_1 R_3} \cos \beta_1}. \quad (9)$$

where R_3 describes the wavelength-selective effect of the grating. The grating feedback is approximately described as a Gaussian function

$$R_3 = R_g \exp\left(-\ln 2 \left(\frac{\lambda - \lambda_0}{\Delta\lambda}\right)^2\right), \quad (10)$$

where $\Delta\lambda$ is about $\lambda/(1.66N)$, and N is the total number of grooves illuminated by the beam [17]. Thus, the modes resonating in the coupled cavity can be expressed as

$$G_0 = G_{ic} G_{ec}(R_3). \quad (11)$$

2.2 Simulation of the oscillation modes

A diode laser array of the Lumibird Corp is used as an example. The array has a wavelength of λ_0 at 808 nm and a spacing of Δp at 400 μm between two adjacent emitters. The optical power is 400 W, and we have simulated nine emitters based on the following parameters [16]: $R_1 = 0.99$, $L_{ic} = 400 \mu\text{m}$, $R_2 = 0.03$, $d^{-1} = 1500 \text{ line/mm}$, $N = 3000$, $R_g = 0.5$, $T_i = 0.99$, $f = 10 \text{ cm}$, $G_m = 1$. To make the emitter work in a stable state, internal cavity modes, external cavity modes, and feedback distribution of the grating must be well matched. According to Eqs. (7), (8), and (10), as visualized in Fig. 3, the mode structure of the central emitter is displayed. It is important to note that the free spectral range of the external cavity is so small (several picometers) that many spectrometers cannot detect it. Therefore, in our simulation, the sampling interval is on the nano-level. The coupled mode of the central emitter (black line) is well locked.

Similarly, the modes of the remaining eight emitters are shown in Fig. 4, in which their center wavelengths are 801.51 nm, 803.14 nm, 804.77 nm, 806.38 nm, 809.60 nm, 811.19 nm, 812.78 nm and 814.36 nm for the -4th , -3rd ,

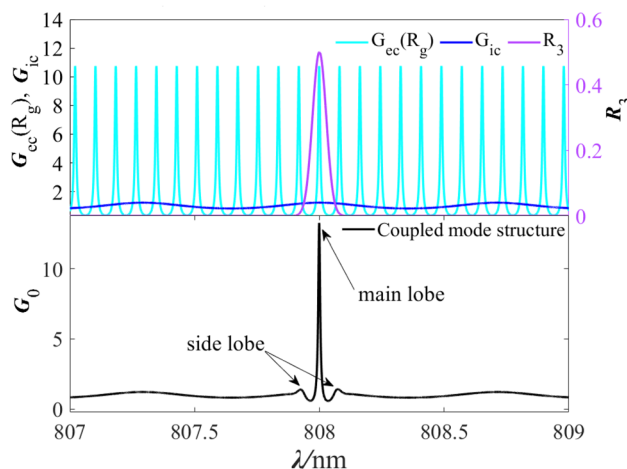


Fig. 3 Modes of the central emitter

-2nd , -1st , 1st , 2nd , 3rd , and 4th emitter. Each mode comprises a main lobe and side (secondary) lobes, with the side lobes getting more visible as the emitter moves away from the central one. As a result, the spectral mode deteriorates from the central emitter to the 4th emitter, mainly because the 4th emitter is further from the central one. Its beam propagates back and forth in the external cavity for a longer time. Moreover, the central emitter’s wavelength of 808 nm matches with the grating, whereas the other 8 emitters’ wavelengths do not match well with the grating selection. Consequently, the external cavity mode cannot well match the internal cavity mode. In addition, the experiment conducted by Xiao also observed secondary peaks in spectral distributions [18]. If there are two peaks in the spectrum, they can compete, causing unstable wavelengths and output power [19].

To assess the modes’ characteristics, a main-side mode ratio is defined as the ratio of side-mode power to main-mode power. Table 1 illustrates that the central emitter has the lowest ratio, while the -4th and 4th emitter ratios are 0.32 and 0.27, respectively, indicating significant side lobe presence. The ratio seems to increase as the emitters move away from the central emitter, making mode competition more likely in these emitters, which is not conducive to single-mode locking.

Figure 5 shows the main-side mode ratios of the diode laser array emitters under different transmittances of the front facet T_2 . A high main-side mode ratio indicates increased competition between modes, potentially resulting in beam crosstalk. Under the same T_2 , the main-side mode ratio of the emitters gradually increases from the center to the edges. This is because the external cavity length of the edge emitters increases compared to the center emitter, and even slight changes in the external cavity length can cause a shift in the external cavity mode,

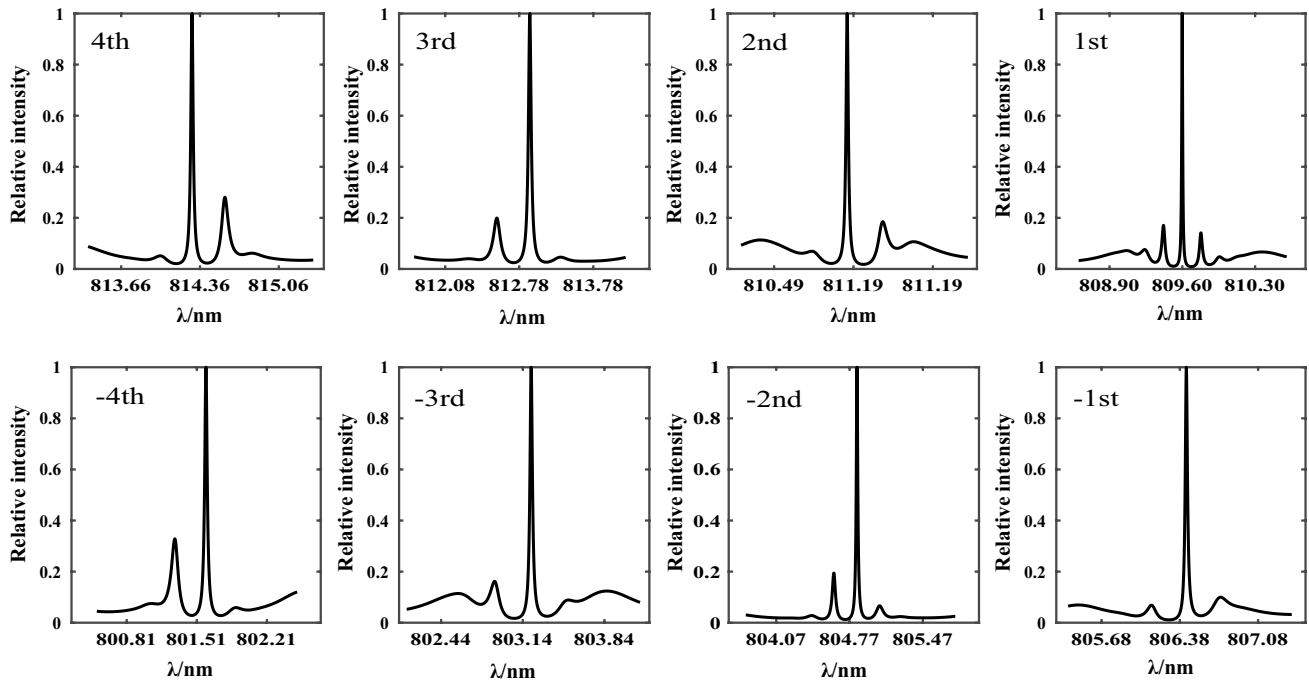


Fig. 4 Oscillation modes of 8 emitters

Table 1 Main-side mode ratios of the nine emitters

The <i>i</i> th emitter	-4th	-3rd	-2nd	-1st	Central	1st	2nd	3rd	4th
Ratios	0.32	0.16	0.19	0.11	0.1	0.17	0.18	0.19	0.27

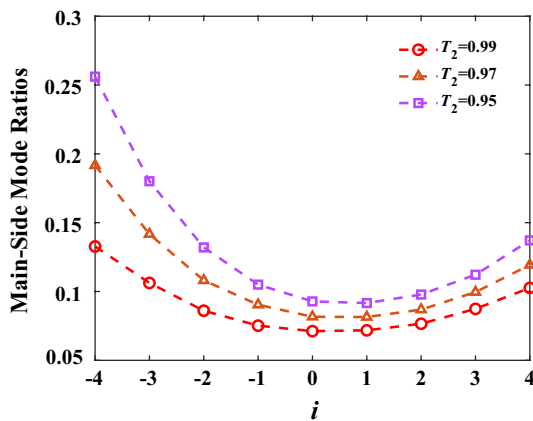


Fig. 5 Main-side mode ratios of the 9 emitters for different transmittances of the front facet T_2

ultimately degrading the coupled cavity mode. As the transmittance of the front facet T_2 decreases, the main-side mode ratios increase, indicating degradation of the coupled cavity mode. This is due to a decrease in the transmittance T_2 , which weakens the impact of the external

cavity feedback effect, making it difficult to achieve effective external cavity feedback [20].

3 Crosstalk theory and beam-combining efficiency analysis

In SBC systems, there are factors such as divergence angles of beams and manufacturing errors of optical components that make it impossible for a beam emitted from an emitter to return perfectly to itself. Instead, it can be fed back into other emitters, resulting in beam crosstalk. This paper examines three cases of beam returning, shown in Fig. 6: (1) self-oscillation means that the main lobe of an emitter is fed back to the emitter itself, which benefits emitter spectrum locking. (2) Self-crosstalk means that the side lobes of an emitter return to the emitter itself, which prevents the main lobe lock and harms the efficiency of SBC. (3) Mutual-crosstalk means that the beam from an emitter is fed back to another emitter, which is common in SBC systems due to the existence of stray lights [10, 21]. The study analyzes the effects of crosstalk on combining efficiency, as both self-crosstalk and mutual-crosstalk impact it.

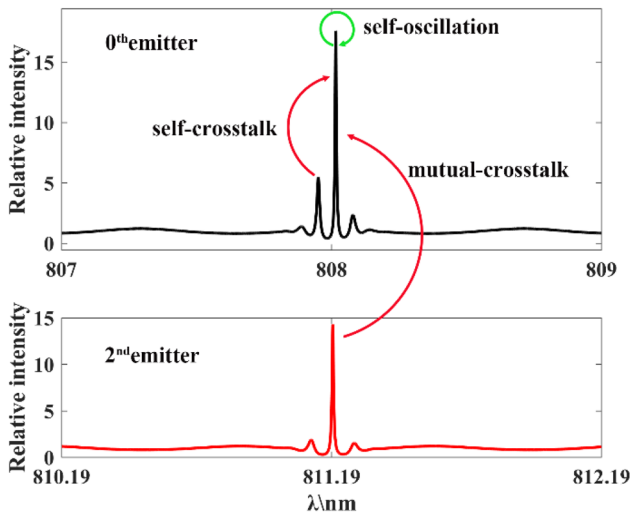


Fig. 6 Schematic of self-oscillation, self-crosstalk, and mutual-crosstalk

3.1 Crosstalk model in SBC systems

The Lang–Kobayashi rate equation is used to describe the effect of crosstalk [5]

$$\frac{d\tilde{E}(t)}{dt} = \frac{1}{2}(1 + \alpha) \left\{ G_N [N(t) - N_0] - \frac{1}{\tau_p} \right\} \tilde{E}(t) + \frac{\kappa}{\tau_d} \tilde{E}(t - \tau) \exp(-i\omega_z \tau_i) + \frac{C_{ii}}{\tau_d} \tilde{E}(t - \tau_i) \exp(-i\omega_z \tau_i) + \frac{C_{ij}}{\tau_d} \tilde{E}(t - \tau_{ij}) \exp(-i\omega_{ij} \tau_{ij}), \tag{12}$$

$$I_{li} = \frac{\left[R\tau_c - N_0 - \frac{1}{G_N \tau_p} + \frac{2\kappa}{G_N \tau_d} \cos(\psi) + \frac{2C_{ii}}{G_N \tau_d} \cos(\psi_z) + \frac{2C_{ij}}{G_N \tau_d} \cos(\psi_{ij}) \right] (1 - R_2) (1 - R_c) T_i T_2 \eta_g \sqrt{\eta_0}}{\frac{\tau_c}{\tau_p} - \frac{2\kappa \tau_c}{\tau_d} \cos(\psi) - \frac{2C_{ii} \tau_c}{\tau_d} \cos(\psi_z) - \frac{2C_{ij} \tau_c}{\tau_d} \cos(\psi_{ij})}. \tag{16}$$

where $\tilde{E}(t)$ is a time-varying plural electric field. The first term on the right side represents the operational properties of the laser. The second, third, and fourth terms refer to self-oscillation, self-crosstalk, and mutual-crosstalk, respectively. C_{ii} and C_{ij} indicate the feedback intensity of the self-crosstalk and the mutual-crosstalk, respectively. C_{ii} represents the ratio of the side lobe peak to the main lobe peak of the i th emitter, while C_{ij} represents the ratio of the main lobe peak of the i th emitter to that of the j th emitter. α refers to the linewidth enhancement factor. G_N is the differential gain factor. N_0 is the carrier density without feedback. κ is equal to $(1 - R_2) \sqrt{R_3/R_2}$. τ_p is the lifetime of a photon. τ_d

is $2nL_{ic}/c$, where n denotes the refractive index of the working medium. ω_i stands for the angular frequency of the i th emitter. ω_z and ω_{ij} represent the angular frequencies of the self-crosstalk beam and mutual-crosstalk beam, respectively. Finally, the round-trip time of the self-crosstalk beam τ_i and that of the mutual-crosstalk beam τ_{ij} in the external cavity are

$$\tau_i = \left[2f + 2\sqrt{f^2 + (i\Delta p)^2} + 2z \right] / c\tau_{ij} = \left[2f + \sqrt{f^2 + (i\Delta p)^2} + \sqrt{f^2 + (j\Delta p)^2} + 2z \right] / c. \tag{13}$$

The equation $\tilde{E}(t) = E(t) \exp[i\psi(t)]$ is substituted into Eq. (12), and then Eq. (14) is obtained as

$$\frac{dE(t)}{dt} = \frac{1}{2} \left\{ G_N [N(t) - N_0] - \frac{1}{\tau_p} \right\} E(t) + \frac{\kappa}{\tau_d} E(t - \tau) \cos(\psi) + \frac{C_{ii}}{\tau_d} E(t - \tau_i) \cos(\psi_z) + \frac{C_{ij}}{\tau_d} E(t - \tau_{ij}) \cos(\psi_{ij}), \tag{14}$$

where $\psi(t) = \omega t + \varphi(t) - \varphi(t - \tau)$, $\psi = \omega_i \tau_i$, $\psi_z = \omega_z \tau_i$, $\psi_{ij} = \omega_{ij} \tau_{ij}$. The rate equation of the carrier density is

$$\frac{dN(t)}{dt} = R - \frac{N(t)}{\tau_c} - G_N [N(t) - N_0] |E(t)|^2, \tag{15}$$

where $R = J/eV$ is the carrier injection rate per unit volume. J is the injected current density. e is the electron charge. V is the volume of the active region. τ_c is carrier lifetime. When the DLA is in a stable state, according to Eqs. (14) and (15), the intensity captured by the coupler is

where η_g is the diffraction efficiency of the grating. R_c is the reflectivity of the coupler. η_0 represents the coupling efficiency of the bidirectional beam within the external cavity. Especially, if the beam crosstalk does not arise ($C_{ii} = C_{ij} = 0$), the optical intensity is

$$I_{0i} = (1 - R_2) \left[R\tau_p - \frac{N_0 \tau_p}{\tau_c} - \frac{1}{G_N \tau_c} \right]. \tag{17}$$

If there is only self-crosstalk ($C_{ij} = 0$) present, and the efficiency is expressed as

$$e_{ii} = \frac{I_{1i}}{I_{0i}} = \frac{\left[R\tau_c - N_0 - \frac{1}{G_N\tau_p} + \frac{2\kappa}{G_N\tau_d} \cos(\psi) + \frac{2C_{ii}}{G_N\tau_d} \cos(\psi_z) \right] (1 - R_c) T_t T_2 \eta_g \sqrt{\eta_0}}{\left[R\tau_c - \frac{N_0\tau_p}{\tau_c} - \frac{1}{G_N\tau_c} \right] \left[\frac{\tau_c}{\tau_p} - \frac{2\kappa\tau_c}{\tau_d} \cos(\psi) - \frac{2C_{ii}\tau_c}{\tau_d} \cos(\psi_z) \right]} \tag{18}$$

Similarly, the efficiency only influenced by the mutual-crosstalk ($C_{ii}=0$) can be written as

$$e_{ij} = \frac{I_{1i}}{I_{0i}} = \frac{\left[R\tau_c - N_0 - \frac{1}{G_N\tau_p} + \frac{2\kappa}{G_N\tau_d} \cos(\psi) + \frac{2C_{ij}}{G_N\tau_d} \cos(\psi_{ij}) \right] (1 - R_c) T_t T_2 \eta_g \sqrt{\eta_0}}{\left[R\tau_c - \frac{N_0\tau_p}{\tau_c} - \frac{1}{G_N\tau_c} \right] \left[\frac{\tau_c}{\tau_p} - \frac{2\kappa\tau_c}{\tau_d} \cos(\psi) - \frac{2C_{ij}\tau_c}{\tau_d} \cos(\psi_{ij}) \right]} \tag{19}$$

The average combining efficiency is calculated as

$$\eta_{SBC} = \frac{\sum_{i=-4}^4 e_{ii} I_{0i}}{\sum_{i=-4}^4 I_{0i}} \tag{20}$$

3.2 Simulation and analysis

Numerical calculations were performed to analyze the impact of beam crosstalk on combining efficiency with the parameters of $\tau_c = 2$ ns, $\tau_p = 3.49$ ps, $N_0 = 2.5 \times 10^{23}/\text{cm}^3$, $V = 1 \times 10^{-16} \text{ m}^3$; $J = 3.125 \times 10^{14} \text{ A/m}^2$, $G_N = 5 \times 10^{-12} \text{ m}^3/\text{s}$, $R_c = 0.15$, $\eta_g = 0.9$, and $\eta_0 = 0.75$ [22, 23]. Figure 7 depicts the variation in the combining efficiency as the transmittance T_2 of the front facet and the reflectivity R_c of the output coupler change. The combining efficiency increases monotonically as the transmittance T_2 increases, while it initially rises slightly and then drops with the increase of reflectivity R_c . A higher T_2 results in lower main-side mode ratios (shown in Fig. 5) and a higher combining efficiency due to suppressed self-crosstalk. In addition, the combining efficiency can also be improved using a coupler with low reflectivity.

Noticeably, one of the purposes of the coupler is to provide necessary optical feedback to the internal cavity, aiding emitters in locking their spectra. Therefore, when designing the reflectance R_c and R_2 of the two important surfaces, it is important to strike a balance between combining efficiency and spectral stability. High combining efficiency necessitates

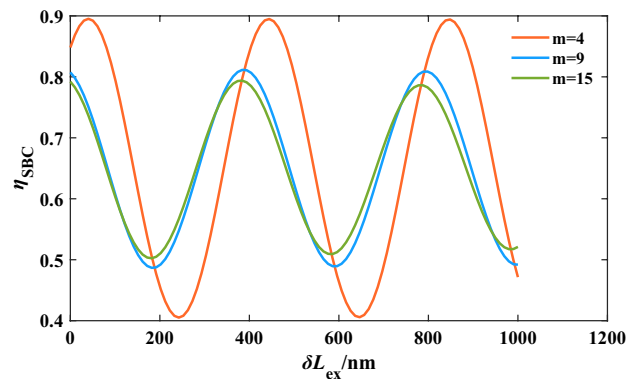


Fig. 8 Variation of combining efficiency with external cavity length

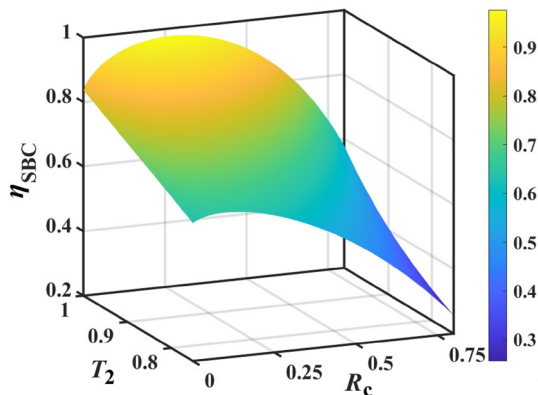


Fig. 7 The combining efficiency affected by the reflectivity of the coupler and the transmittance of the front facet

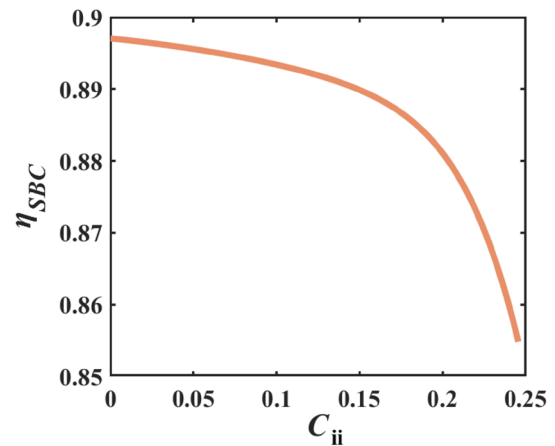


Fig. 9 Effect of the self-crosstalk on the combining efficiency

a small R_c , but ensuring spectral stability requires it to be greater than R_2 [24].

Figure 8 plots the change of combining efficiency η_{SBC} with the external cavity length for varying total numbers of emitters (the total number of emitters is $2m + 1$. For example, if $m = 4$, the diode laser array would contain a total of 9 emitters). It can be seen from Fig. 8 that the combining efficiency η_{SBC} exhibits periodic variation, as the output intensity of the single-emitter diode laser also varies periodically with the external cavity length. This periodic behavior indicates that external cavity diode lasers share similarities with conventional laser cavities. Each curve has a period of approximately 400 nm, which is nearly half the central wavelength of 808 nm. As the number of emitters increases, the peak value of combining efficiency gradually decreases, and the fluctuation amplitude becomes smaller. The SBC using a laser array with fewer emitters results in a larger efficiency fluctuation range and is more sensitive to the external cavity length. For laser arrays with more emitters, the difference

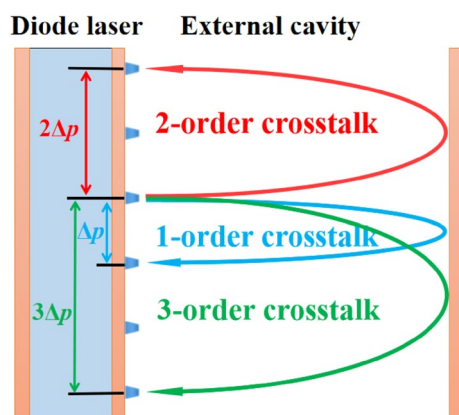


Fig. 10 Multi-order crosstalk

between the peak and valley values is smaller, thus requiring less strict external cavity length adjustment.

Figure 9 depicts the impact of self-crosstalk on combining efficiency. The effect of self-crosstalk on combining efficiency is not significant. When the self-crosstalk factor increases from 0 to 0.2, there is a decrease in efficiency of approximately 1.7%. As the factor C_{ii} grows from 0 to 0.25, the combining efficiency decreases from 89.7 to 85.5%. Since C_{ii} is influenced by the intensity of the side lobes, suppressing side lobes can enhance the combining efficiency. Figure 5 demonstrates that the spectral mode's side lobe can be improved through raising the transmittances T_2 of the front facet. In other words, methods such as coating anti-reflection films on the front facet can effectively control the self-crosstalk. It is important to note that the self-crosstalk factor generally remains below 0.15. A value exceeding the limit of 0.2 indicates the diode emitter's wavelength is poorly locked, which in turn, causes a rapid decline in combining efficiency and could lead to system failure.

In comparison, effect of mutual-crosstalk on combining efficiency is analyzed next. Figure 10 illustrates the multi-order crosstalk. Figure 11a gives the mutual-crosstalk between the central emitter (the 0 emitter) and another emitter (the 1st, 2nd, 3rd or 4th emitter). Figure 11b illustrates the crosstalk between any two emitters except for the central one. The curve 1-0 in Fig. 11a denotes the mutual-crosstalk between the 1st emitter and the central emitter, referred to as 1-order crosstalk (the two emitters with a spacing Δp). Similarly, the curve 3-0 denotes the mutual-crosstalk between the 3rd emitter and the central emitter, or 3-order crosstalk (the two emitters with a spacing $3\Delta p$). The curve 4-0 represents 4-order crosstalk. The same applies to Fig. 11b. In Fig. 11a, the crosstalk occurs between the central and the other emitters. The combining efficiency degrades severely due to the mutual-crosstalk deterioration. The 1-0 curve falls the quickest among the three curves, causing combining efficiency

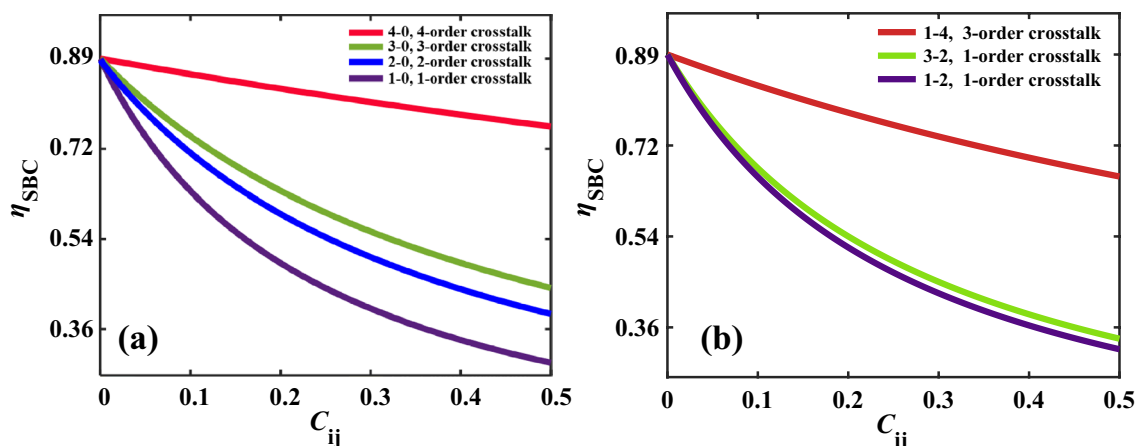


Fig. 11 Effect of the mutual-crosstalk on the combining efficiency

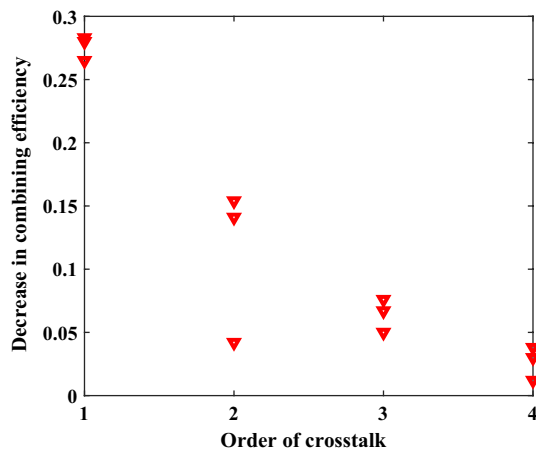


Fig. 12 Effect of multi-order crosstalk on combining efficiency

to drop from 89.7 to 27.1%. Whereas curve 3-0 decreases from 89.7 to 44%, and curve 4-0 shows the slowest fall from 89.7 to 79%. This suggests that the combining efficiency is most adversely affected by the 1-order crosstalk, which is attributed to the distance between the 1st emitter and the central emitter is the closest. Equation (3) demonstrates that when contrasted with the 3rd and 4th emitters, the center wavelength of the 1st emitter is the nearest to that of the central emitter. Thus, the 1-order crosstalk easily engages in mode competition, which consumes inverted particles and reduces luminous efficiency. Figure 11b suggests that 1-order crosstalk has a more severe impact on efficiency than 3-order crosstalk. From Figs. 9 and 11, it is evident that the mutual-crosstalk has a greater impact on combining efficiency when compared to self-crosstalk. Therefore, it is important to suppress mutual-crosstalk, especially between two adjacent emitters, and it can be achieved by reducing the divergence angles of beams, increasing the gap between the beams, and using an aperture before the coupler [21].

The impact of multi-order crosstalk on combining efficiency is assessed. To obtain the decrease in combining efficiency caused by multi-order crosstalk, the curves in Fig. 11 were linearly fitted. In Fig. 12, the horizontal axis lists the order of mutual-crosstalk and the vertical axis shows the decrease in combining efficiency. For example, the crosstalk occurring between two adjacent emitters (the 1-order crosstalk) is represented by 1 on the horizontal axis, and the 2-order crosstalk happened between two emitters with a spacing of $2\Delta p$ is denoted by 2. The 4-order crosstalk makes a decline in combining efficiency of about 3%, while the 1-order crosstalk results in a reduction of roughly 27%. It can be seen that the mutual-crosstalk between two adjacent emitters has a significant effect on the combining efficiency. As the distance between two crosstalk emitters grows, crosstalk's effect on combining efficiency gradually decreases. Experimental results from Professor Tang's

team at Huazhong University of Science and Technology also indicated that low-order crosstalk has a greater impact on the beam-combining system [25].

4 Conclusion

In SBC systems, various factors including beam divergence angles, lens aberration, grating fabrication errors, and secondary diffraction of the grating can cause stray beams to appear in the external cavity. If these stray beams are fed back to the DLA, it can harm the emitters' ability to lock their spectra, leading to a decrease in combining efficiency. Based on gain functions, locked spectral modes of emitters are simulated and analyzed in detail. The results show that the mode structures of emitters have side modes, with the side lobe becoming more prominent as the emitter moves away from the central emitter and mode competition potentially arising. Applying anti-reflection film on the emitting surface of the DLA can suppress the side lobes of the spectra. Then, based on the spectral mode, beam crosstalk is divided into self-crosstalk and mutual-crosstalk. Using the Lang–Kobayashi rate equations, a theoretical model for crosstalk is proposed to analyze the combining efficiency. In order to maintain both the combining efficiency and the spectral stability, it is necessary to optimize the reflectivity of the coupler to be greater than the back facet of the DLA. The combining efficiency fluctuates periodically as the external cavity length increases. For SBC systems with more emitters, the amplitude of efficiency fluctuation is smaller, and adjustment of the cavity length does not need to be more precise. In addition, compared to self-crosstalk, mutual-crosstalk has a significantly negative impact on combining efficiency. The low-order crosstalk in mutual-crosstalk makes the combining efficiency drop more seriously.

Acknowledgements The research is sponsored by Department of Science and Technology of Sichuan Province [2021ZYD0036], National Natural Science Foundation of China [61905203].

Author contributions Zhen Wu wrote the full text of the article. Wei Cai calculated and drew the Fig. 3 to 12. Chengshuang Yang, Qingsong Zhang and Zairu Ma checked and revised the article. Yinghao Zhuang draw the Fig. 1 and 2, and check the theoretical equations.

Declarations

Conflict of interest The author declare that they have no conflict of interest.

References

1. M. Iwaya, S. Tanaka, T. Omori, K. Yamada, R. Hasegawa, M. Shimokawa, A. Yabutani, S. Iwayama, K. Sato, T. Takeuchi,

- S. Kamiyama, H. Miyake, Recent development of UV-B laser diodes. *Jpn. J. Appl. Phys.* **61**(4), 040501 (2022). <https://doi.org/10.3584/1347-4065/ac3be8>
2. B. Niu, X. Shi, K. Ge, J. Ruan, Z. Xu, S. Zhang, D. Guo, T. Zhai, An all-optical tunable polymer WGM laser pumped by a laser diode. *Nanoscale Adv.* **4**(9), 2153–2158 (2022). <https://doi.org/10.1039/D2NA00025C>
 3. C. C. Cook, T. Y. Fan, Spectral beam combining of Yb-doped fiber lasers in an external cavity. In *Advanced Solid State Lasers*. Optica Publishing Group, PD5 (1999). <https://doi.org/10.1364/ASSL.1999.PD5>
 4. Z. Wu, Z. Zhong, L. Yang, B. Zhang, Beam properties in a spectral beam combining system based on trapezoidal multilayer dielectric gratings. *JOSA B.* **33**(2), 171–179 (2016). <https://doi.org/10.1364/JOSAB.33.000171>
 5. R. Lang, K. Kobayashi, External optical feedback effects on semiconductor injection laser properties. *IEEE J. Quantum Electron.* **16**(3), 347–355 (1980). <https://doi.org/10.1109/JQE.1980.1070479>
 6. L. Yang, Z. Wu, Z. Zhong, B. Zhang, Effect of crosstalk on combined beam characteristics in spectral beam combining systems. *Opt. Commun.* **384**, 30–35 (2017). <https://doi.org/10.1016/j.optcom.2016.09.060>
 7. E.J. Bochove, Theory of spectral beam combining of fiber lasers. *IEEE J. Quantum Electron.* **38**(5), 432–445 (2002). <https://doi.org/10.1109/3.998614>
 8. Z. Wu, L. Yang, Z. Zhong, B. Zhang, Influence of laser array performance on spectrally combined beam. *J. Mod. Opt.* **63**(19), 1972–1980 (2016). <https://doi.org/10.1080/09500340.2016.1183056>
 9. A.K. Goyal, A. Sanchez, G.W. Turner, T.Y. Fan, Z.L. Liao, M.J. Manfra, P.J. Foti, L. Missaggia, P. O'Brien, J.L. Daneu, Wavelength beam combining of mid-IR semiconductor lasers. *IEEE Lasers Electro-Opt. Soc.* **2**, 532–533 (2001). <https://doi.org/10.1109/LEOS.2001.968924>
 10. H. Meng, T. Sun, H. Tan, J. Yu, W. Du, F. Tian, J. Li, S. Gao, X. Wang, D. Wu, High-brightness spectral beam combining of diode laser array stack in an external cavity. *Opt. Express* **23**(17), 21819–21824 (2015). <https://doi.org/10.1364/OE.23.021819>
 11. A. Sevia, O. Andrusyak, I. Ciapurin, G. Venus, L. Glebov, Spectral beam combining with volume Bragg gratings: cross-talk analysis and optimization schemes. *SPIE.* **6216**, 243–254 (2006). <https://doi.org/10.1117/12.666024>
 12. W. Zhang, P. Cao, F. Ting, X. Zhou, W. Zheng, High-efficiency spectral beam combining of an individual laser diode bar with polarization multiplexing. *Opt. Lett.* **48**(4), 1080–1083 (2023). <https://doi.org/10.1364/OL.483315>
 13. Z. Zhu, W. Wu, L. Wang, Y. Hui, H. Lei, Q. Li, Dual-wavelength laser source by spectral beam combining of two Nd: YAG pulse lasers. *Appl. Opt.* **62**(8), 1939–1942 (2023). <https://doi.org/10.1364/AO.481107>
 14. X. Fan, J. Zhang, S. Li, S. Li, Y. Wang, F. Du, X. Huang, Y. Li, L. Zhang, C. Wang, A method to achieve spectral beam combining based on a novel symmetric grating. *Front. Phys.* **10**, 1280 (2022). <https://doi.org/10.3389/fphy.2022.1102323>
 15. J. Zhang, H. Peng, J. Zhang, J. Wang, J. Han, Y. Lei, L. Qin, L. Wang, Spectral beam combining of diode lasers extended into the non-SBC direction. *Opt. Express.* **30**(19), 33733–33738 (2022). <https://doi.org/10.1364/OE.468586>
 16. H. Gong, Z. Liu, Y. Zhou, W. Zhang, T. Lv, Mode-hopping suppression of external cavity diode laser by mode matching. *Appl. Opt.* **53**(4), 694–701 (2014). <https://doi.org/10.1364/AO.53.000694>
 17. G.Y. Yan, A.L. Schawlow, Measurement of diode laser characteristics affecting tunability with an external grating. *JOSA B.* **9**(11), 2122–2127 (1992). <https://doi.org/10.1364/JOSAB.9.002122>
 18. Y. Xiao, F. Brunet, M. Kanskar, M. Faucher, A. Wetter, N. Holehouse, 1-kilowatt CW all-fiber laser oscillator pumped with wavelength-beam-combined diode stacks. *Opt. Express* **20**(3), 3296–3301 (2012). <https://doi.org/10.1364/OE.20.003296>
 19. D. Chen, Z. Fang, H. Cai, J. Geng, R. Qu, Instabilities in a grating feedback external cavity semiconductor laser. *Opt. Express* **16**(21), 17014–17020 (2008). <https://doi.org/10.1364/OE.16.017014>
 20. Q. Zhang, Z. Wu, W. Cai, Y. Zhuang, Y. She, Spectral-combined beam characteristics based on external cavity feedback diode laser array. *Opt. Eng.* **62**(5), 056101–056101 (2023). <https://doi.org/10.1117/1.OE.62.5.056101>
 21. D. Ott, S.N.S. Reihani, L.B. Oddershede, Crosstalk elimination in the detection of dual-beam optical tweezers by spatial filtering. *Rev. Sci. Instrum.* **85**(5), 053108 (2014). <https://doi.org/10.1063/1.4878261>
 22. F.A. Memon, F. Morichetti, Z.A. Arain, U.A. Korai, A. Melloni, Semiconductor laser in distributed optical feedback regime. *Wireless Pers. Commun.* **106**, 2149–2161 (2019). <https://doi.org/10.1007/s11277-018-5931-y>
 23. G. Haiping, W. Chenhao, W. Fei, Z. Lijing, X. Chengwen, Study on the dynamic mode stability of grating-feedback external cavity diode lasers. *Laser Phys.* **26**(4), 045002 (2016). <https://doi.org/10.1088/1054-660X/26/4/045002>
 24. C.E. Hamilton, S.C. Tidwell, D. Meekhof, J. Seamans, N. Gitkind, D.D. Lowenthal, High-power laser source with spectrally beam-combined diode laser bars. *SPIE High-Power Diode Laser Technol. Appl.* **II**(5336), 1–10 (2004). <https://doi.org/10.1117/12.531595>
 25. Y. Song, X. Yu, C. Hu, P. Wang, H. Ma, X. Tang, Analysis of crosstalk in spectral beam combining of diode laser bar. *Appl. Opt.* **61**(12), 3390–3399 (2022). <https://doi.org/10.1364/AO.456640>

Publisher's Note Springer Nature remains neutral with regard to jurisdictional claims in published maps and institutional affiliations.

Springer Nature or its licensor (e.g. a society or other partner) holds exclusive rights to this article under a publishing agreement with the author(s) or other rightsholder(s); author self-archiving of the accepted manuscript version of this article is solely governed by the terms of such publishing agreement and applicable law.